Low Temperature Plasma Technology Laboratory

**Quiescent and Unstable Regimes
of a Helicon Plasma**

Max Light, F. F. Chen, and P.L. Colestock
*Los Alamos National Laboratory
and UCLA Electrical Engineering Department*

LTP-108   August, 2001
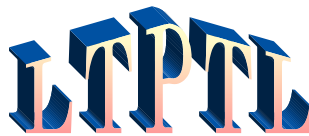
Electrical Engineering Department
Los Angeles, California 90095-1594

UNIVERSITY OF CALIFORNIA • LOS ANGELES

Quiescent and unstable regimes of a helicon plasma

Max Light†, F F Chen‡ and P L Colestock†

† Los Alamos National Laboratory, Los Alamos, NM, USA
‡ Department of Electrical Engineering, University of California, Los Angeles, Los Angeles, CA, USA

E-mail: `mlight@lanl.gov`

Abstract. Known for their ability to produce high densities at low power, helicon discharges have found many uses. However, it has been discovered that the plasma density saturates, and even falls for light ion gases, as the magnetic field is increased. Detailed measurements of fluctuations in plasma density reveal the onset of a strong, low frequency electrostatic instability. This onset correlates well with density saturation and is predicted from a linear theory.

1. Introduction

Radio-frequency (rf) plasma sources based on helicons are noted for their unusually high ionization efficiency. These sources are used in plasma processing of semiconductors, ionospheric plasma research, ion lasers, general plasma physics experiments, and plasma thruster research [1, 2, 3, 4, 5, 6].

Helicon discharge sources have, for the most part, been considered relatively quiescent up to their operating limit in magnetic field and input power. The only recurrently reported exceptions were the neutral depletion effect [7, 8] and relaxation oscillations [9]. Neutral depletion can be avoided through proper design of the plasma chamber, while relaxation oscillations are avoided with optimal antenna/plasma rf coupling. Thus, depending on the power available to the magnetic field coils and rf amplifier, a monotonic increase in plasma density n_0 with magnetic field strength B_0 was expected.

Sakawa *et al* [10] have reported that the plasma density in this discharge does not monotonically increase with magnetic field strength in light gases. This has also been observed in several other helicon experiments [11, 12, 13, 14]. Efforts to increase the maximum attainable plasma density in these sources are driven by their applicability to such areas as space propulsion. Arguably the most important characteristic of magnetized plasma sources is the scaling of equilibrium density with magnetic field strength $n_0(B_0)$, and understanding the physics behind this trend is critical.

This work presents experimental evidence of a low frequency instability prevalent above different static magnetic field strengths in different gases. Above these critical magnetic field strengths B_{crit} for each gas, very strong density fluctuations were observed as well as a non-monotonic behavior in $n_0(B_0)$. The measured B_{crit} values are thus seen to serve as a demarcation from quiescent to unstable equilibrium behavior in this helicon plasma.

2. Experimental apparatus

Investigation of the $n_0(B_0)$ scaling was performed on the apparatus shown in figure 1 [15], with magnetic field strength ≤ 1.5 kG and 2 kW of 13.56 MHz power into a right-helical [16] antenna. Gas fill pressure was kept constant at 8 $mTorr$. Characterization of fluctuations was done by measuring the magnitude and phase of density and floating potential fluctuations $(\tilde{n}, \tilde{\phi})$ with a triple-probe technique employed in magnetic fusion [17, 18]. Density fluctuations were measured by biasing a probe tip well into the ion saturation regime. All measurements were taken 30 cm downstream of the antenna mid-plane, unless specified otherwise.

3. Measurements

Ion density measurements, given in figure 2 for all gases used in this experiment, revealed the characteristic interruption in the monotonic increase of $n_0(B_0)$ reported on other experiments. Note that the light ion gases (hydrogen and helium) are peaked, while the heavier gases (neon and argon) tend to saturate or show a dramatic decrease in the slope of $n_0(B_0)$ above their respective B_{crit} values.

The lower hybrid (LH) resonance has been offered as a candidate for the characteristic $n_0(B_0)$ profile [19, 20], and figure 3 shows the relationship between B_{crit} and the LH magnetic field B_{LH} at the location of the measurement. For the high plasma densities in this experiment, B_{LH} is well approximated by the high density limit of the lower hybrid frequency ω_{LH} as

$$B_{LH} = \frac{\omega_{LH} \left(m_p m_e\right)^{1/2}}{e} \, A^{1/2} \qquad (1)$$

where m_p, m_e, and e correspond to the ion mass, electron mass, and electron charge respectively, and the driving frequency is substituted for ω_{LH}. B_{crit} is seen to vary approximately as $A^{1/5}$, and correlation with B_{LH} is weak at best. The lower hybrid resonance is a function of the *local* n_0 and B_0 as well as the electron and ion masses, and collisions can significantly suppress the resonance. In fact, for most experiments including this one, fill pressure and ionization percentage are such that neutral and Coulomb collision frequencies can be greater than the driving frequency at the antenna. Detailed theory shows that the LH resonance is not to be expected here, and indeed the data do not support this explanation.

Waveforms of the ion saturation current for $0 \leq B_0 \leq 1.5 kG$, along with their respective Fourier transforms, are given in figures 4 and 5 for helium. It became apparent that two different regimes of the equilibrium plasma existed. In the first region, where $B_0 < B_{crit}$, density fluctuations $\tilde{n}$ were either non-existent or of high frequency and very weak. The frequencies decreased with increasing B_0, a behavior characteristic of drift waves. These well known waves [21, 22, 23, 24, 25, 26] have a frequency given by

$$\omega_{de} = k_\theta \frac{KT_e}{eB_0} \frac{\nabla n_0}{n_0} \qquad (2)$$

where k_θ corresponds to the azimuthal wave-number. The second region, where $B_0 \geq B_{crit}$, showed very strong $\tilde{n}$ fluctuations ($\tilde{n}/n_0 \approx 0.2$) at very low frequencies. These frequencies remained relatively constant as B_0 was increased. The behavior of the plasma in the region above B_{crit} was reported previously [20], and subsequently hypothesized to be a result of the LH resonance. However, as pointed out earlier, the data were not consistent with the existence of an LH resonance.

Figure 6 shows a spectrogram of $\tilde{n}(B_0)$ in neon along with $n_0(B_0)$. Note that the saturation in plasma density and onset of strong, low-frequency fluctuations in $\tilde{n}$ occur at the same B_{crit}. This correlation was seen in all gases used in the experiment, and B_{crit} increased with increasing ion mass. Figure 7 shows the magnitude of the dominant

low frequency component of $\tilde{n}$ fluctuations in helium, illustrating the onset of strong low-frequency fluctuations that continue to grow past $B_{crit} \approx 760G$.

Figures 8 and 9 give equilibrium radial profiles of space potential V_s and n_0 respectively above and below B_{crit} in helium. While the density profile remained relatively unchanged with B_0, it was clear that $V_s(r)$ did show changes with B_0. In particular, the $E_0 \times B_0$ drift changes with radius differently at each B_0. Shear in the $E_0 \times B_0$ drift is a trigger for an azimuthal Kelvin-Helmholtz instability [29, 30, 31, 32].

Figures 10 and 11 also show the radial profiles of $\tilde{n}/n_0$ and $\tilde{\phi}/T_e$ in helium. Below B_{crit}, $\tilde{n}/n_0$ and $\tilde{\phi}/T_e$ are extremely weak. For $B_0 > B_{crit}$, the fluctuations are very strong with significant off-axis peaks. In figure 11 the maximum in $\tilde{\phi}/T_e$ corresponds to the location where $V_s(r)$ deviates significantly from flat for $B_0 = 850$ G, while it has two peaks at $B_0 = 1000$ G. The first again corresponds to the significant deviation in $V_s(r)$ and the second lies near the outer edge of the plasma. A co-location of maxima in $E_0 \times B_0$ velocity and $\tilde{\phi}/T_e$ is a characteristic signature of the azimuthal Kelvin-Helmholtz instability [31]. Note also in figure 10 the locations of the maximum in $\tilde{n}/n_0$ for $B_0 > B_{crit}$. These are situated just beyond the location of the greatest $|\nabla n_0|$ (figure 8). Peaks in $\tilde{n}/n_0$ near the maximum in $|\nabla n_0|$ are characteristic of the resistive drift instability [23].

4. Theory summary

The instability threshold can be predicted from a two fluid model employing the usual linear perturbation technique [33] to describe the fluctuating quantities $\tilde{n}$ and $\tilde{\phi}$ in a slab geometry, and has been detailed elsewhere [15]. Collision rates were dominated by neutrals. Ions were assumed to be at room temperature, thus eliminating magnetic viscosity effects; electron inertia was neglected; fluctuations were assumed to be electrostatic ($\beta \ll 1$ for this experiment) and were Fourier-analyzed in the θ (y) and z directions; wave-particle resonance effects were neglected; and the density $n_0(x)$ and space potential $V_s(x)$ profiles were allowed to vary; this effectively includes both resistive drift and Kelvin-Helmholtz mechanisms. Perturbations had the form $exp[i(m\theta + k_z z - \omega t)]$, and were assumed to be absolute, with k_z real and $\omega = \omega_R + i\gamma_I$ complex. The detected fluctuations had ω small enough to justify the ordering

$$\omega, \omega_{EB}(x), \omega_*(x) \ll \Omega_c \tag{3}$$

where the $E_{0x} \times B_{0z}$ drift, electron diamagnetic drift, and ion cyclotron frequencies are defined respectively by

$$\omega_{EB}(x) = k_y v_E(x) = k_y \frac{V_s'(x)}{B_0}$$

$$\omega_*(x) = k_y \frac{KT_e}{eB_0} \frac{n_0'(x)}{n_0(x)}; \quad \Omega_c = \frac{eB_0}{M_i} \quad . \tag{4}$$

In the above equations, k_y is the azimuthal wave-number; x corresponds to the radial coordinate in a slab geometry; and $'$ denotes $\partial/\partial x$.

Significant ion temperatures have been discovered in a helicon source [2]. This would seem to conflict with assigning $T_i = 0$ in the present study. However, a comparison of the pressure and collision terms in the ion momentum equation shows that the collision term dominates at both equilibrium and first order for the parameter regime of this experiment.

Coupling the linearized equations of motion and continuity for each species in a singly ionized plasma via the plasma approximation $n_i = n_e$ results in a quartic dispersion relation

$$0 = \frac{\hat{\omega}}{C_s^2}\left(\frac{-\omega_* \nu_e + ik_z^2 v_{th}^2}{\hat{\omega}\nu_e + ik_z^2 v_{th}^2}\right) + \frac{(k_x^2 + k_y^2)(\hat{\omega} + i\nu_i)}{\Omega_c(\Omega_c + v_E')}$$

$$-\frac{ik_x n_0'/n_0(\hat{\omega} + i\nu_i)}{\Omega_c(\Omega_c + v_E')} + \frac{k_y n_0'/n_0}{\Omega_c + v_E'} - \frac{k_z^2}{\hat{\omega} + i\nu_e}$$

$$+\frac{i2k_x k_y v_E'(\hat{\omega} + i\nu_i)^2}{\Omega_c^2(\Omega_c + v_E')^2} - \frac{2k_y^2 v_E'(\hat{\omega} + i\nu_i)}{\Omega_c(\Omega_c + v_E')^2} \quad , \tag{5}$$

where ν_j is the collision rate for each species, v_{th} the electron thermal velocity, C_s the ion sound speed, and $\hat{\omega} = \omega - \omega_{EB}$ the doppler shifted eigenfrequency. The appropriate root was identified as the low frequency branch having a positive imaginary part. In the limit of a flat radial space potential profile and no ion collisions it was seen to be the resistive drift wave [21, 22, 15]. Addition of a non-zero space potential profile adds the possibility of a shear in the $E_0 \times B_0$ radial profile as mentioned earlier.

Equation 5 yields the local frequency and growth rate for a given set of measured equilibrium profiles $n_0(x), V_s(x)$, and parameters B_0, T_e, and M_i. Measured frequencies were consistent with theory. The growth rate versus B_0 is given in figure 7 for all gases used in the experiment.

5. Discussion and conclusions

From the helium data, figures 8 and 9 show that the energy to drive an instability is available from $|\nabla n_0(r)|$ and $|\nabla V_s(r)|$, corresponding to the resistive drift and Kelvin-Helmholtz mechanisms respectively. Resistive drift waves are to be expected in almost any discharge of this type, where radial gradients in n_0 exist. They may be present at $B_0 < B_{crit}$ as relatively weak fluctuations in $\tilde{n}$ in the range $\approx 10 kHz$, but do not have a large effect on the plasma equilibrium. Significant off-axis gradients in $V_s(r)$ appear here for all but the lowest B_0, enabling an azimuthal Kelvin-Helmholtz instability. Thus, the unstable equilibrium of the plasma appears to be an admixture of the two, whereas the quiescent region can have small amplitude drift waves present.

In figure 7 the predicted growth rate in helium significantly decreases while the measured amplitude of $\tilde{n}/n_0$ continues to grow. This discrepancy is due to the linear nature of the theoretical model. It is appropriate for characterizing instability onset, but is not accurate for prediction in the strongly saturated regime. Furthermore, the strong low frequency component in the spectrogram of figure 6 has a signature that

changes slightly above the onset at B_{crit}. This is most likely a characteristic of the strongly saturated regime as well. Figure 12 shows the magnetic field strengths for maxima in the predicted instability growth rate in each gas, saturation in $n_0(B_0)$, and onset of strong low frequency fluctuations B_{crit} for each gas. This gives clear evidence of correlation between the instability and equilibrium behavior in the helicon plasma. We have, therefore, found that the saturation of $n_0(B_0)$ correlates with the onset of a low-frequency instability at B_{crit}, a demarcation between relatively quiescent and unstable plasma regimes, whose value is predicted with a linear theory.

Acknowledgments

References

[1] M. A. Liebermann and R. A. Gottscho in G. Hass, editor, *Physics of Thin Films* (Academic, New York, 1994).

[2] E. E. Scime, P. A. Keiter, M. W. Zintl, M. M. Balkey, J. L. Kline, and M. Koepke, Plasma Sources Sci. Technol., **7**, 186 (1998).

[3] P. Zhu and R. W. Boswell, Phys. Rev. Lett., **63**, 2805 (1989).

[4] B. N. Breizman and A. V. Arefiev, Phys. Rev. Lett., **84**, 3863 (2000).

[5] F. F. Chen and D. D. Blackwell, Phys. Rev. Lett., **82**, 2677 (1999).

[6] F. R. Chang Diaz, J. P. Squire, R. D. Bengston, B. N. Breizmann, F. W. Baity, and M. D. Carter, in *Proceedings of the 36th AIAA/ASME/ASEE Joint Propulsion Conference*, No. 2000-3756 (2000).

[7] J Gilland, R Breun, and N Hershkowitz, Plasma Sources Sci. Technol., **7**, 416 (1998).

[8] D. G. Miljak and F. F. Chen, Plasma Sources Sci. Technol., **7**, 537 (1998).

[9] A.W. Degeling, T.E. Sheridan, and R. W. Boswell, Physics of Plasmas, **6**, 1641 (1999).

[10] Y. Sakawa, T. Takino, and T. Shoji, Phys. Plasmas, **6**, 4759 (1999).

[11] A.J. Perry and R.W. Boswell, J. Vac. Sci. Technol. B, **9**, 310 (1991).

[12] J.H. Kim and H.Y. Chang, Phys. Plasmas, **3**, 1462 (1996).

[13] P.A. Keiter, E.E. Scime, and M.M. Balkey, Phys. Plasmas, **4**, 2741 (1997)

[14] D.A. Schneider, D.D. Borg, and I.V. Kamenski, Phys. Plasmas, **6**, 703 (1999).

[15] M. Light, F.F. Chen, and P.L. Colestock, Phys. Plasmas, **8**, 4675 (2001).

[16] M. Light and F.F. Chen, Phys. Plasmas, **2**, 1084 (1995).

[17] J.M. Beall, Y.C. Kim, and E.J. Powers, J. Appl. Phys., **53**, 3933 (1982).

[18] E.J. Powers, Nucl. Fusion, **14**, 749 (1974).

[19] S. Yun, J. Kim, and H. Chang, J. Vac. Sci. Technol. A, **15**, 673 (1997).

[20] J.G. Kwak, S.K. Kim, and S. Cho, Phys. Lett. A, **267**, 384 (2000).

[21] F.F. Chen, Phys. Fluids, **4**, 1448 (1961).

[22] F.F. Chen, Phys. Fluids, **10**, 1647 (1967).

[23] H.W. Hendel, T.K. Chu, and P.A. Politzer, Phys. Fluids, **11**, 2426 (1968).

[24] T.K. Chu, B. Coppi, H.W. Hendel, and F.W. Perkins, Phys. Fluids, **12**, 203 (1969).

[25] R.F. Ellis, E. Marden-Marshall, and R. Majeski, Plasma Phys., **22**, 113 (1980).

[26] N. D'Angelo and R.W. Motley, Phys. Fluids, **6**, 422 (1963).

[27] H. Lashinsky, Phys. Rev. Lett., **12**, 121 (1964).

[28] L.G. Schlitt and H.W. Hendel, Phys. Fluids, **15**, 1578 (1972).

[29] G.I. Kent, N.C. Jen, and F.F. Chen, Phys. Fluids, **12**, 2140 (1969).

[30] D.L. Jassby, Phys. Rev. Lett., **25**, 1567 (1970).

[31] D.L. Jassby, Phys. Fluids, **15**, 1590 (1972).

[32] F.W. Perkins and D.L. Jassby, Phys. Fluids, **14**, 102 (1971).

[33] N.A. Krall and A.W. Trivelpiece, *Principles of Plasma Physics*, (Freemann, San Francisco, 1986).

Figure captions

Figure 1. Experimental apparatus. The magnetic field was uniform to within a few percent over the length specified by the dashed arrow. The chamber diameter was 15.2 cm, and the overall length 1.97 m. The left end of the chamber is non magnetic stainless steel 11 cm in length.

Figure 2. Electron density on axis versus B_0 for all gases used in the experiment (from [15]).

Figure 3. Lower hybrid, B_{LH}, and critical, B_{crit}, magnetic fields as a function of ion mass number A. Points are B_{crit} for $A = 1$ (H), $A = 4$ (He), $A = 20$ (Ne), $A = 40$ (Ar), and $A = 131$ (Xe). Solid line corresponds to $B_{LH}(A)$, and the dashed line is a best power fit to the B_{crit} data. Xenon was run at 5 mT fill pressure.

Figure 4. $B_0 < B_{crit}$. (a) Time and (b) frequency domain waveforms of the signal to a probe biased to $-100V$ at $r = 2$ cm in helium.

Figure 5. $B_0 > B_{crit}$. (a) Time and (b) frequency domain waveforms of the signal to a probe biased to $-100V$ at $r = 2$ cm in helium. Note the difference in scale from figure 4

Figure 6. Spectrogram of $\tilde{n}$ fluctuations in neon (from [15]). A probe biased to -100 V was placed at $r = 2.5$ cm. $n_0(B_0)$ is given below. $H = -7.1 dBm$ and $L = -24.1$ dBm.

Figure 7. Growth rate γ_I versus B_0 for various gases (solid lines). Parameters used for the calculation were: $k_x = k_y = 30/m, k_z = 0.25/m$, electron/neutral collision frequency $= 10^7$, ion/neutral collision frequency $= 10^3$, plasma density profile was represented as $n'_0/n_0 = 1/a$ where a $=$ plasma radius, $V'_s(r)$ and $V''_s(r)$ were represented as $1/L_1$ and $1/L_1 \times 1/L_2$ respectively, $L_1 = 6.7 \times 10^{-3}$, and $L_2 = 0.01$. Also shown is $\tilde{n}/n_0$ (points connected by dashed line) for helium.

Figure 8. Space potential radial profiles below and above B_{crit}. Points are measured data and lines are smoothed fits to each data set.

Figure 9. Electron density radial profiles below and above B_{crit}.

Figure 10. $\tilde{n}/n_0$ radial profiles below and above B_{crit}.

Figure 11. $\tilde{\phi}/T_e$ radial profiles below and above B_{crit}.

Figure 12. Measured magnetic field strengths corresponding to the saturation or significant deviation from a monotonic increase in $n_0(B_0)$ (filled triangles), onset of strong low frequency fluctuations in $\tilde{n}$ (open circles), and predicted maximum growth rate (open squares) versus atomic mass number A.

30 cm

Left column (Volts vs mS): 1425 G, 1350 G, 1000 G, 900 G, 800 G

Right column (dB vs kHz): 1425 G, 1350 G, 1000 G, 900 G, 800 G

n_0 $(10^{13}$ $cm^{-3})$

r (cm)

1000 G

850 G

600 G

300 G

$\phi^{\sim}/T_e$

0.8

0

0   2   4   6

r (cm)

1000 G

850 G

600 G

300 G